

THE FERMI-GBM X-RAY BURST MONITOR: THERMONUCLEAR BURSTS FROM 4U 0614+09

M. LINARES^{1,7}, V. CONNAUGHTON², P. JENKE^{3,8}, A. J. VAN DER HORST⁴, A. CAMERO-ARRANZ^{5,9}, C. KOUVELIOTOU³, D. CHAKRABARTY¹, E. BEKLEN¹⁰, P. N. BHAT², M. S. BRIGGS², M. FINGER⁵, W. S. PACIESAS⁵, R. PREECE², A. VON KIEHLIN⁶, C. A. WILSON-HODGE³

Accepted for publication in The Astrophysical Journal.

ABSTRACT

Thermonuclear bursts from slowly accreting neutron stars (NSs) have proven difficult to detect, yet they are potential probes of the thermal properties of the neutron star interior. During the first year of a systematic all-sky search for X-ray bursts using the Gamma-ray Burst Monitor (GBM) aboard the *Fermi Gamma-ray Space Telescope* we have detected 15 thermonuclear bursts from the NS low-mass X-ray binary 4U 0614+09, when it was accreting at nearly 1% of the Eddington limit. We measured an average burst recurrence time of 12 ± 3 d (68% confidence interval) between March 2010 and March 2011, classified all bursts as normal duration bursts and placed a lower limit on the recurrence time of long/intermediate bursts of 62 d (95% confidence level). We discuss how observations of thermonuclear bursts in the hard X-ray band compare to pointed soft X-ray observations, and quantify such bandpass effects on measurements of burst radiated energy and duration. We put our results for 4U 0614+09 in the context of other bursters and briefly discuss the constraints on ignition models. Interestingly, we find that the burst *energies* in 4U 0614+09 are on average between those of normal duration bursts and those measured in long/intermediate bursts. Such a continuous distribution in burst energy provides a new observational link between normal and long/intermediate bursts. We suggest that the apparent bimodal distribution that defined normal and long/intermediate *duration* bursts during the last decade could be due to an observational bias towards detecting only the longest and most energetic bursts from slowly accreting NSs.

Subject headings: X-rays: bursts — binaries: close — X-rays: individual (4U 0614+09) — stars: neutron — X-rays: binaries — accretion, accretion disks

1. INTRODUCTION

Matter accreted onto neutron stars (NSs) in low-mass X-ray binaries (LMXBs) piles up and settles into the NS envelope. After a period accumulating fuel, thermonuclear reactions become unstable and the accreted layer ignites, producing a thermonuclear flash (also known as type I X-ray burst, “burst” hereafter; Grindlay et al. 1976; Maraschi & Cavaliere 1977). During the thermonuclear runaway all or part of the accreted hydrogen (H) and/or helium (He) are converted into heavier elements so that fresh fuel needs to accumulate before the next burst occurs, giving rise to a cyclic behavior. This has been observed in many thermonuclear burst sources (“bursters”) that alternate short bursts (typically seconds- to minutes-long) with extended periods of

persistent accretion-powered emission (typically hours-days; see Lewin et al. 1993; Strohmayer & Bildsten 2006, for reviews). The persistent luminosity, L_{pers} , often expressed as a fraction of the Eddington limit, is thought to trace the mass accretion rate per unit surface area, \dot{m} . When the \dot{m} history is known, the time spanned between two successive bursts (known as burst wait time, t_{wait}) determines how much mass needs to be piled up until the ignition conditions are met at the base of the accreted layer. When data gaps prevent the detection of successive bursts a more convenient parameter is the wait time averaged over the available observations, i.e., the ratio between total accumulated exposure time and number of bursts detected, which we refer to as burst recurrence time, t_{rec} .

The vast majority of thermonuclear bursts observed during more than three decades, referred to as *normal bursts*, last between a few seconds and a few minutes and radiate between 10^{38} erg and a few times 10^{39} erg (e.g., Galloway et al. 2008). In the last decade two new classes of bursts have emerged: *long/intermediate bursts* (long duration bursts or simply “long bursts”; e.g., in’t Zand et al. 2005), which last tens of minutes and radiate 10^{40} – 10^{41} erg; and *superbursts*, which last for hours up to more than a day and radiate energies of the order of 10^{42} erg (Cornelisse et al. 2000; Kuulkers 2004; Chenevez et al. 2008). As more long bursts have been discovered, the question was raised of whether they form a distinct population of bursts or they constitute a rare, extremely long and energetic case of normal bursts.

Long bursts take place preferentially when \dot{m} is low,

¹ Massachusetts Institute of Technology - Kavli Institute for Astrophysics and Space Research, Cambridge, MA 02139, USA

² University of Alabama in Huntsville, Huntsville, AL 35899, USA

³ Space Science Office, VP62, NASA/Marshall Space Flight Center, Huntsville, AL 35812, USA

⁴ Astronomical Institute ‘Anton Pannekoek’, University of Amsterdam, 1090 GE Amsterdam, the Netherlands

⁵ Universities Space Research Association, Huntsville, AL 35805, USA

⁶ Max Planck Institute for Extraterrestrial Physics, Giessenbachstrasse, Postfach 1312, 85748 Garching, Germany

⁷ NWO Rubicon Fellow

⁸ NASA Postdoctoral Program Fellow

⁹ Current address: Institut de Ciències de l’Espai (IEEC-CSIC), Campus UAB, Fac. de Ciències, Torre C5, parell, Barcelona, 08193, Spain

¹⁰ Physics Department, Suleyman Demirel University, 32260 Isparta, Turkey

near or below 1% of the Eddington rate, thus their properties depend on the nuclear burning processes at work at the lowest accretion rates, where sedimentation of heavy elements may play a role (Peng et al. 2007). Furthermore, ignition of long bursts takes place deep in the envelope after a thick layer of fuel is built up. Hence their properties are also sensitive to the heat flowing from the crust, providing an independent method to study the thermal properties of the NS interior (Cumming et al. 2006). We refer hereafter to bursts occurring when \dot{m} is close to or lower than 1% of the Eddington limit as *low- \dot{m} bursts*, with the understanding that these include both normal and long duration bursts.

4U 0614+09 harbors a slowly and persistently accreting NS (active since its discovery, Giacconi et al. 1972) and belongs to the sub-class of low luminosity NS-LMXBs (the so-called atoll sources, Hasinger & van der Klis 1989). The system is likely an ultracompact binary, based on the optical-to-X-ray flux ratio (van Paradijs & McClintock 1994; Juett et al. 2001), tentative orbital periodicities (O’Brien et al. 2005; Shahbaz et al. 2008) and its low but persistent X-ray luminosity (in’t Zand et al. 2007). However, the exact nature and composition of the (likely degenerate) donor star has been a matter of debate (although strong constraints have been placed from X-ray and optical spectroscopy; Juett et al. 2001; Nelemans et al. 2004; Werner et al. 2006).

Although 4U 0614+09 is a known burster (Swank et al. 1978; Brandt et al. 1992) and a frequently observed source, a relatively small number of bursts have been recorded from 4U 0614+09 since its discovery four decades ago. Only two bursts were detected with the *Rossi X-ray Timing Explorer* (RXTE) despite numerous observations over the course of 16 yr (which amount to more than 2 Msec of on-source exposure time). A compilation of these and 31 other bursts detected with several X-ray observatories was presented by Kuulkers et al. (2010, K10 hereafter). They found two long duration bursts during 2001–2002 with integrated radiated energies $E_b \gtrsim 4 \times 10^{40}$ erg, when the persistent soft X-ray luminosity was steady, and an increased normal burst rate after that period with the corresponding t_{rec} in the 9–14 d range.

The scarcity of bursts detected from 4U 0614+09 or similar systems is not surprising. Low- \dot{m} bursts are expected to recur on timescales much longer than the observing windows of pointed X-ray telescopes, which typically observe LMXBs with little or no interruptions for up to about a day. Hence detection with pointed instruments is rare and both t_{wait} and t_{rec} have remained poorly constrained. Thanks to its very large instantaneous field of view ($\simeq 10$ sr) and its sensitivity to X-ray photon energies down to 8 keV, the Gamma-ray Burst Monitor (GBM; Meegan et al. 2009) on board the *Fermi Gamma-ray Space Telescope* is able to detect rare, bright and short-lived X-ray bursts. This is of particular relevance to the study of thermonuclear bursts from accreting NSs. A dedicated search using wide-field X-ray monitors provides the most efficient way to measure accurately the recurrence time of low- \dot{m} bursts. With this goal, we started on 2010 March 12 a systematic GBM all-sky search for X-ray bursts, as described in Section 2. We report 15 thermonuclear bursts from 4U 0614+09

collected during the first year of our campaign, between 2010 March 12 and 2011 March 12. We present the burst properties and accretion rate history in Section 3. In Section 4 we discuss these results, quantify bandpass effects on the observed burst properties (Section 4.1) and compare 4U 0614+09 to other low- \dot{m} bursters (Section 4.2). Section 5 summarizes our main findings and conclusions.

2. DATA ANALYSIS

2.1. GBM all-sky search for X-ray bursts

GBM is an all sky monitor whose primary objective is to extend the energy range over which gamma-ray bursts (GRBs) are observed in the Large Area Telescope (LAT) on Fermi (Meegan et al. 2009). The twelve sodium iodide (NaI) scintillation detectors cover an energy range from 8 keV to 1 MeV. Due to the spacecraft’s 50 degree rocking angle, exposure of the sky is essentially uniform throughout the current search period between 2010 March 12 and 2011 March 12. The X-ray burst search uses the first 3 channels (8–50 keV) of CTIME data from the NaI detectors. Periods where the spacecraft is performing a rapid maneuver ($> 2.75 \times 10^{-3}$ rad/s), SAA passages, GRBs and contaminating features, such as solar events, that prevent a good background model fit are removed from the data. An empirical background model which includes Earth occultations of bright sources is fit to the data. Short-lived (~ 10 –1000 s) X-ray flares are selected by visually inspecting the CTIME Channel 1 data (12–25 keV) along with the fitted background model. Using the first three channels, a preliminary localization is obtained using the cosine differential response of the detectors (see Sec. 2.2). If the χ^2 of the localization is less than 450, the localization is more than 10° or 3σ away from the Sun and the position lies above and more than 1σ from the Earth’s limb (a 66° radius circle around the geocenter), the selected feature is considered an X-ray burst candidate and set aside for further analysis. We define the observing duty cycle as the ratio between the time when the source was visible to GBM (excluding times of Earth occultation, rapid slews and SAA passages) and the total time spanned by the current search (one year). In the case of 4U 0614+09, the duty cycle was 49.3% and the total effective exposure time 180 d.

In order to optimize the signal-to-noise ratio (S/N) in the X-ray bursts from 4U 0614+09 and measure the burst timescales and peak count rate, we extracted background-corrected 12–25 keV light curves adding the three brightest detectors, using daily CTIME data rebinned to 1s time resolution. We defined the burst rise time t_{rise} as the time for the resulting intensity to increase from 25% to 90% of its peak value. We interpolated linearly between data points and we estimate an uncertainty of 0.5s (half the time resolution used) in t_{rise} . We used CSPEC light curves in the 8–15 keV band keeping the original 4s time resolution in order to measure the duration of the bursts, defining the burst end as the time when the intensity drops below 10% of the peak.

2.2. Localization

The 12 NaI detectors are thin disks with different orientations. Using the known angular response of the detectors, the relative count rates registered during a burst in the 12 detectors provide a solution for the likely arrival direction of the burst. The measured count rates

TABLE 1
GBM X-RAY BURSTS FROM 4U 0614+09.

ID	Peak time (UTC)	Detectors ^a n(°)	Peak rate ^b (c/s)	R.A. (°)	DEC (°)	Error (°)
B1	2010-03-28 00:16:13	9(22) 0(42) 1(44) 10(45) 2(59)	381±37	98.4	4.6	3.4
B2	2010-04-29 03:46:49	1(22) 2(26) 0(45) 5(59)	617±41	92.6	8.5	6.0
B3	2010-05-18 10:56:59	4(29) 5(32) 3(50)	360±37	95.0	4.4	9.3
B4	2010-05-25 07:35:59	1(14) 0(19) 3(46) 5(57) 2(59)	595±40	104.6	1.4	6.8
B5	2010-07-05 05:08:03	5(16) 1(43) 2(51) 3(55) 0(60)	593±41	87.8	6.6	5.5
B6	2010-07-29 07:12:47	1(26) 2(29) 5(39) 0(50)	496±39	99.0	10.5	8.2
B7	2010-08-09 09:30:02	4(17) 3(36) 5(46)	740±43	87.9	10.1	2.9
B8	2010-09-10 18:20:15	3(14) 4(33) 5(60)	489±35	96.7	15.2	4.5
B9	2010-10-12 03:54:43	10(37) 2(37) 9(46) 1(47)	311±34	94.9	13.7	6.2
B10	2010-10-21 09:33:42	7(23) 6(32) 3(42) 8(46) 4(60)	596±41	94.3	9.6	3.5
B11	2010-11-28 03:50:45	9(27) 10(30) 11(41)	668±40	97.0	12.0	4.1
B12	2011-01-11 20:29:51	9(18) 11(44) 10(45) 6(51) 7(54)	490±39	87.0	6.8	3.6
B13	2011-01-14 15:26:50	9(27) 11(36) 10(40) 7(59)	302±36	97.7	18.4	9.7
B14	2011-01-18 22:47:38	7(12) 6(17) 9(50) 0(57) 8(57) 11(60)	627±41	98.5	13.2	10.4
B15	2011-01-24 11:00:23	9(22) 10(31) 11(46)	716±42	89.8	9.4	7.8

^aList of detectors pointing within 60° of 4U 0614+09 at the time of the burst, used for spectral analysis (Sec. 2.3). The angular distance from each detector to 4U 0614+09 is given between parenthesis, in degrees. Only detectors with pointing offsets $\leq 50^\circ$ were used to extract the light curves.

^bNet 12–25 keV count rate from the three brightest detectors.

are compared with model rates for arrival directions on a 1° resolution grid measured in the spacecraft coordinate frame. A χ^2 -minimization algorithm finds the best match for the observed rates to 41168 positions on the sky, with an uncertainty that depends on how steeply χ^2 increases away from the minimum. In order to make the assessment of the goodness-of-fit independent of the intensity of the burst, the observed rates are first normalized to a fiducial “average” burst before calculating χ^2 . This reduces the χ^2 values for very bright bursts with low statistical uncertainties where the systematic errors dominate, and allows us to use one χ^2 value to reject poor fits to the data over the range of burst intensities detected by GBM.

Because the angular response is energy-dependent, a source spectrum is folded through the response when calculating the model rates. The model rates in the search for X-ray bursts are calculated at energies below 50 keV and compared to count rates measured in the corresponding CTIME channels. To maximize the signal in the search for these events, the counts in CTIME channels 0 through 2 are used, and the model rates are evaluated between 8 and 50 keV. The uncertainties in the detector responses below 10 keV and the noisier background at the lowest energies may introduce larger systematic errors than incurred above 10 keV, so the localization is also performed in the 10–50 keV energy band. By default the search for X-ray bursts uses a power-law model rate function with an index of 2, which represents a variety of phenomena but may not be the best model for type I X-ray bursts. Model rates for a softer power-law function with index 3 were therefore used at the localization stage once the X-ray burst candidates were isolated in the overall data set. Model rates with a blackbody spectrum that was later shown to be a good fit to the X-ray burst candidates were subsequently generated and used to see whether a good model fit produced a better localization.

As expected, the statistical error on the localization was higher by about 1° for a given model when the rates below 10 keV were excluded from the localization

of the 15 events associated with 4U 0614+09. The error on the localization, inferred from the distance to the known source position, was comparable for localizations performed using both energy ranges. The ratio between the offset from the source and the statistical uncertainty suggests that the systematic error on the localizations using the 8–50 keV energy range may be larger, with 41% (82%) contained within the 1(2) σ uncertainty region compared to 54% (87%) for the localizations performed in the 10–50 keV energy range. The centroids (weighting each position by its statistical uncertainty) of the 15 combined locations are between 0.5°–1.1° from 4U 0614+09 for the 10–50 keV range localizations depending on the model, with the more representative softer power-law and blackbody spectral models yielding centroids at 0.5 and 0.6° from the source. The blackbody and softer power-law models produced localizations that were on average closer to the source by about 0.7° compared to the power-law model with index of -2. The 8–50 keV localizations produce a centroid that lies between 1.6 and 1.9° from the source. Within the relatively low (15) number of events available, our results suggest that systematic errors may be larger when the full energy range is used to localize events. Whilst our analysis suggests that using the 10–50 keV energy range with either a soft power-law or black-body model produces the best results when localizing type I X-ray bursts using GBM data, the events are weak enough that the uncertainties are dominated by statistics, and these systematic effects are small by comparison.

2.3. Spectral analysis

We performed time-averaged and time-resolved spectroscopy of the 15 confirmed bursts from 4U 0614+09. We used the continuous CSPEC data type in our analysis, with the best available spectral resolution for GBM and 4 s time resolution (Meegan et al. 2009). The data were analyzed with the RMFIT (3.3rc8) software package which has been developed for the GBM data analysis. The time-varying background was fitted with polynomial functions of the third or fourth order. We generated De-

tector Response Matrices using GBMRSP V1.9. In our analysis we used all the NaI detectors with zenith angles to the source smaller than 60° , and which view was not obstructed by the solar panels or other parts of the spacecraft.

We have fitted the time-integrated spectra with a power law and a blackbody function, using the Castor statistic (C-stat)¹¹, and in all bursts a blackbody provided the best fit to the data. The difference in C-stat between the two models ranges from several tens to hundreds, illustrating the improvement of a thermal model over a power law. To quantify this and estimate the significance of the blackbody fit improvement over the power law fit, we simulated 10^4 spectra from the best-fit model parameters. We found that for a typical value ($\simeq 40$) of the difference in C-stat between thermal and power law model fits, the fit improvement is significant at the $>99.99\%$ (3.9σ) confidence level. Since these events are spectrally very soft for the GBM energy band, we used the 8–30 keV range in our analysis, but we note that using the full NaI energy range gives consistent results. We also checked spectral fits from individual detectors and they all give consistent results. Here we use the results obtained by combining the appropriate detectors to maximize the S/N.

2.4. Persistent emission and mass accretion rate

In order to characterize the soft and hard persistent (accretion-powered) X-ray emission from 4U 0614+09 and estimate \dot{m} , we used 1.5–12 keV light curves collected by the All-Sky Monitor (ASM; Levine et al. 1996) on board the *Ross X-ray Timing Explorer* as well as 15–50 keV light curves from *Swift*'s Burst Alert Telescope (BAT; Barthelmy et al. 2005), using data from the hard X-ray transient monitor (Krimm et al. 2006). We used ASM and BAT daily intensity measurements taken between 2010 March 12 and 2011 March 12 including all available (2σ) detections, which amount to 81% and 76% of the whole one-year period for ASM and BAT, respectively.

As we are interested for the purpose of this work in long-term (weeks to months) changes in \dot{m} as well as its mean value over the search period, we applied a running average with a 12-d window to the resulting light curves. At the expense of disregarding variability on timescales of less than $\simeq 2$ weeks, this method increases the S/N and removes short data gaps due to, e.g., high background in ASM or BAT. The window length was chosen to prevent data gaps from affecting the running average, while keeping a relatively short window. We then converted the ASM and BAT intensity into 2–20 keV and 20–100 keV luminosity, respectively, using WebPimms¹² and a distance to 4U 0614+09 of 3.2 kpc (K10). We assumed that the X-ray spectrum of 4U 0614+09, averaged over its spectral states (Linares 2009), is well represented by a power law model with photon index 2. The resulting 2–100 keV luminosity gives an estimate of the bolometric persistent luminosity, L_{pers} , which we convert into \dot{m} assuming that all the gravitational energy is radiated away

isotropically at the surface of a 10 km radius, $1.4 M_\odot$ mass NS (this and other assumptions may result into uncertainties in \dot{m} of a factor ~ 2 ; see, e.g., discussion in Coriat et al. 2012). When normalizing L_{pers} by the Eddington luminosity (L_{Edd}) we use a fiducial value of $2.5 \times 10^{38} \text{ erg s}^{-1}$, yet we note that the exact value depends on the composition of the accreted material. Using $3.8 \times 10^{38} \text{ erg s}^{-1}$, a value more typical of H-poor material, does not change our results and conclusions.

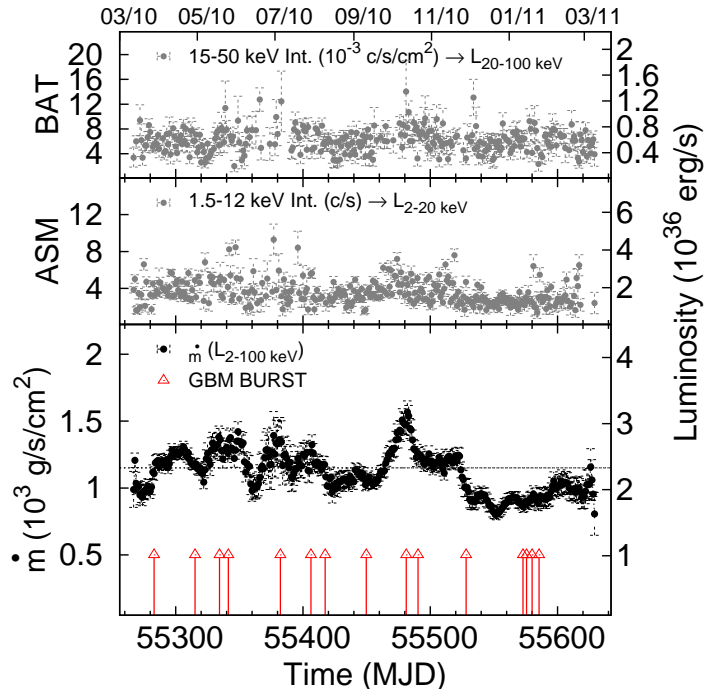


FIG. 1.— *Bottom panel:* Evolution of mass accretion rate per unit surface (left axis) derived from the 2–100 keV persistent luminosity (right axis) after applying a 12-d window running average (see Sec. 2.4 for details). Red arrows along bottom axis show the times of the 15 thermonuclear bursts from 4U 0614+09 detected with GBM during the 1 yr period. Month start dates are marked along the top axis, from March 2010 to March 2011. *Top & middle panels:* Hard (BAT) and soft (ASM) X-ray light curves of 4U 0614+09. Daily-averaged intensity measurements (left axes) are converted into luminosity (right axes).

3. RESULTS

We found a total of 15 X-ray bursts from 4U 0614+09 during the first year of our *Fermi*-GBM X-ray burst search (Sec. 2.1). Only 33 bursts had been observed from 4U 0614+09 since it was discovered, using observations taken over 32 yr by 8 different X-ray observatories (between 1975 and 2007; see K10). Therefore, the 15 GBM bursts presented herein constitute a substantial improvement in burst detection rate. Table 1 shows all GBM bursts labeled in chronological order B1–B15, their peak times, count rates and locations. All bursts were clearly detected in the 12–25 keV band with all GBM NaI detectors pointing within 60° of 4U 0614+09, and none of them was detected above 50 keV, as expected for thermonuclear bursts given their thermal spectrum. Figure 1 shows the burst times as well as the soft (ASM) and hard (BAT) X-ray light curves of 4U 0614+09. From these, we obtained the 2–100 keV persistent luminosity and in-

¹¹ A modification of Cash's C-statistic used to fit spectra with low number of counts, which tends to χ^2 for large number of counts; <http://heasarc.gsfc.nasa.gov/docs/xanadu/xspec/wstat.ps>

¹² Portable Interactive Multi-Mission Simulator v. 4.5 at <http://heasarc.gsfc.nasa.gov/Tools/w3pimms.html>

TABLE 2
PROPERTIES OF THE GBM TYPE I X-RAY BURSTS FROM
4U 0614+09.

ID	kT_{peak} (keV)	L_{peak} (10^{38} erg/s)	E (10^{39} erg)	Rise (s)	Duration (s)	Δt (d)
B1	2.7 ± 0.1	1.79 ± 0.07	2.07 ± 0.01	1.6	28.6	—
B2	3.0 ± 0.1	1.65 ± 0.05	1.77 ± 0.02	2.2	20.3	32.1
B3	2.9 ± 0.2	0.89 ± 0.07	0.72 ± 0.03	0.9	29.4	19.3
B4	2.9 ± 0.1	1.75 ± 0.05	1.06 ± 0.03	1.2	11.1	26.2
B5	2.6 ± 0.1	1.97 ± 0.07	2.33 ± 0.12	1.5	26.0	40.9
B6	3.1 ± 0.1	1.28 ± 0.06	0.82 ± 0.02	1.1	16.4	24.4
B7	3.2 ± 0.1	2.72 ± 0.06	5.77 ± 0.03	4.5	46.5	35.2
B8	3.0 ± 0.1	1.91 ± 0.05	4.19 ± 0.03	1.8	44.0	32.4
B9	2.7 ± 0.1	1.38 ± 0.06	2.23 ± 0.02	1.3	34.1	31.4
B10	3.0 ± 0.1	2.36 ± 0.09	2.15 ± 0.06	1.5	20.7	9.2
B11	3.2 ± 0.1	2.17 ± 0.07	2.84 ± 0.03	2.8	30.5	37.8
B12	3.0 ± 0.1	1.89 ± 0.08	2.58 ± 0.05	0.9	49.0	44.7
B13 ^b	3.3 ± 0.2	0.74 ± 0.05	0.43 ± 0.02	1.3	10.1	2.8
B14	2.9 ± 0.1	2.05 ± 0.08	1.49 ± 0.07	2.9	14.0	4.3
B15	3.2 ± 0.1	2.30 ± 0.08	1.82 ± 0.08	3.1	15.0	5.5

^aBurst peak luminosity L_{peak} and radiated energy E at 3.2 kpc. Rise time, duration and E as measured by GBM, not corrected for bandpass. Δt is the time in days since the previous burst from 4U 0614+09 detected by GBM (not corrected by on-source exposure time and therefore corresponds to an upper limit on the burst wait time, t_{wait} ; Sec. 1).

^bDue to the low number of counts per spectrum, blackbody temperature and radius are strongly correlated in B13. If we fix the radius to a value of 5 km, consistent with all other bursts, the peak temperature becomes $kT_{\text{peak}} \simeq 2.5$ keV.

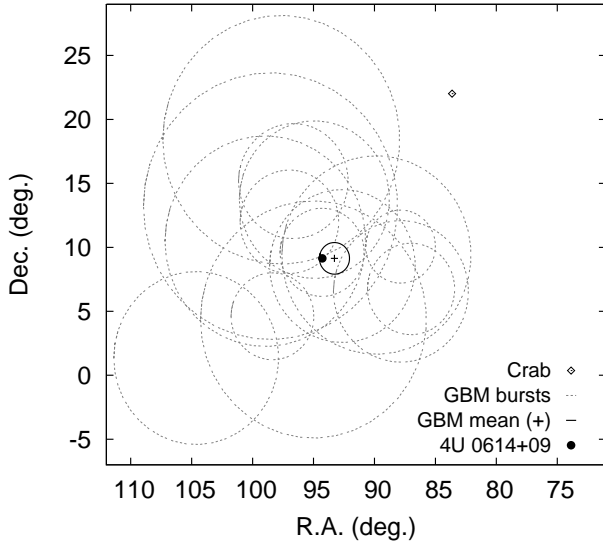


FIG. 2.— GBM localizations of the 15 bursts from 4U 0614+09 presented in this work (gray dashed circles show 1σ error circles; see Section 2.2 and Table 1). The average position from all GBM bursts (black open circle), the known position of 4U 0614+09 (black filled circle; Migliari et al. 2006) and the closest bright X-ray source (Crab, black diamond) are also shown.

ferred mass accretion rate per unit area \dot{m} (Sec. 2.4), which remained between 0.6% and 1.3% of the Eddington limit (L_{Edd} and \dot{m}_{Edd} , respectively; Sec. 2.4) during the whole period studied in this work, with an average value $\langle L_{\text{pers}} \rangle = 2.3 \times 10^{36}$ erg s⁻¹ ($\dot{m}/\dot{m}_{\text{Edd}} = 0.9\%$). All the *RXTE* observations taken between March 2010 and March 2011 showed 4U 0614+09 in the intermedi-

ate state, where it remains most of the time (the accretion state intermediate between spectrally hard and soft states; see, e.g., Linares 2009).

As shown in Figure 2, the burst locations are consistent with the known position of 4U 0614+09. For about 90% of the bursts the 2σ confidence region around the best location includes 4U 0614+09 (see full details in Section 2.2). All bursts are more than 10° and 70° away from the center of the Sun and Earth, respectively, as seen from the *Fermi* spacecraft (Sec. 2.1). The closest known bright X-ray source (Crab) and burster (4U 0513-40) are about 16° and 51° away, respectively, and there is no known LMXB within 15° of 4U 0614+09. This, together with the thermonuclear nature of the bursts (see below), allows us to identify all bursts B1–B15 as coming from 4U 0614+09.

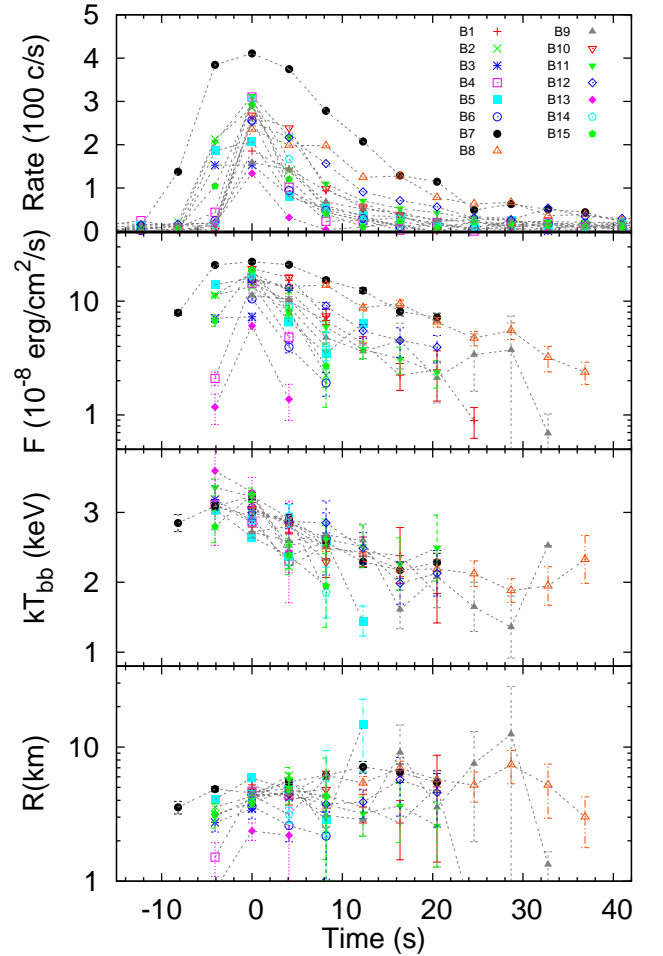


FIG. 3.— Time-resolved spectroscopy of the GBM X-ray bursts from 4U 0614+09, showing (from top to bottom): net count rate, bolometric flux, blackbody temperature and blackbody radius. The temperature decay is clearly visible, identifying all bursts as thermonuclear.

We first performed power law fits to the time-averaged 8–30 keV spectrum of all bursts and obtained photon indices in the 3–4.4 range. Such high values of the photon index reveal a relatively steep or “soft” spectrum, indicative of thermal emission. Indeed, a blackbody model gives a better fit (Sec. 2.3) to the average spectrum of all

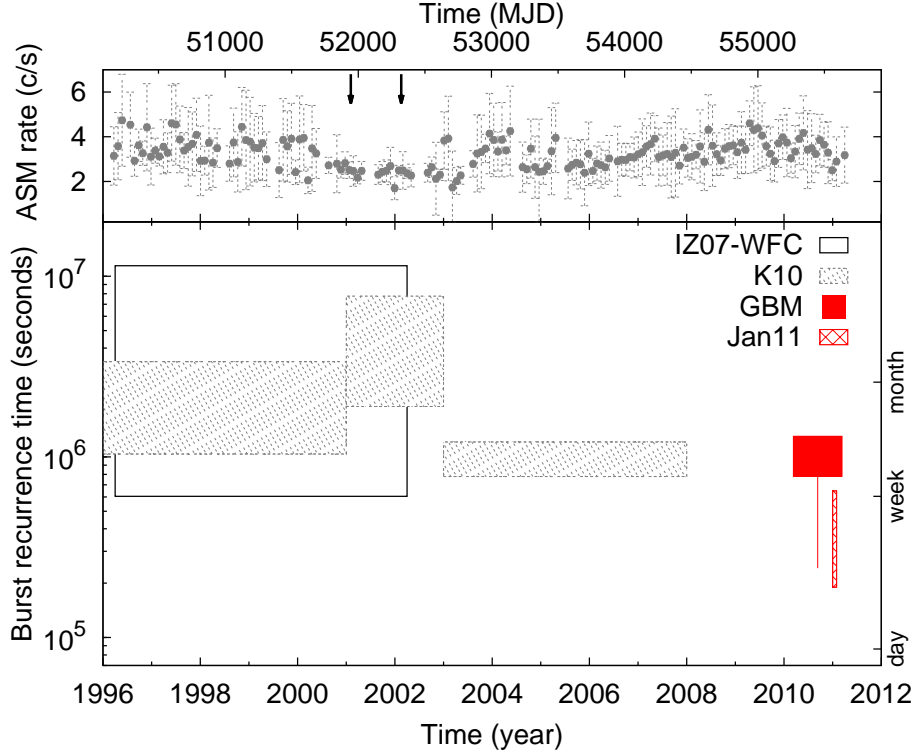


FIG. 4.— *Bottom*: Measurements of burst recurrence time t_{rec} in 4U 0614+09, between 1996 and 2012. The red filled rectangle shows our measurement of t_{rec} from the first year of the GBM all-sky X-ray burst search. The red vertical error bar marks the shortest wait time, 2.8 d, and the crossed red rectangle shows the t_{rec} measured in January 2011. Gray dashed rectangles display the limits on t_{rec} found by K10. The solid open black rectangle shows the WFC limits on t_{rec} for 4U 0614+09 (from in’t Zand et al. 2007). All t_{rec} ranges shown with rectangles are 1σ confidence intervals assuming a Poisson distribution. *Top*: Mission-long *RXTE*-ASM light curve of 4U 0614+09, showing monthly weighted averages of the 1.5–12 keV intensity. Error bars display ± 1 standard deviation, highlighting the lower long-term variability 2001–2002 period discussed by K10, when the two long bursts were detected (their times are marked with arrows along the top axis).

bursts, yielding temperatures in the 2.5–2.8 keV range, fully consistent with a thermonuclear origin. The results of the time-resolved spectroscopy (Sec. 2.3) are shown in Figure 3, and confirm the thermonuclear nature of the bursts. We detect in all cases a significant drop in burst temperature along the decay, also referred to as “cooling tail”. This is a defining property of type I X-ray bursts and a sufficient condition to identify bursts as thermonuclear. Burst peak temperatures (kT_{peak}) are in the range 2.6–3.3 keV (Table 2), and decay to $\simeq 2$ keV in the latest detected stages of the bursts.

We use throughout this work the 3.2 kpc distance found by K10 from the brightest photospheric radius expansion (PRE) burst in their sample. The apparent blackbody radii that we find (Figure 3; between $\simeq 3$ km and $\simeq 10$ km during most phases of the bursts) are consistent with previously reported values for 4U 0614+09 (K10) and compatible with the expected NS emitting area (note that no gravitational redshift or spectral corrections have been applied to these values; see, e.g., Lewin et al. 1993). All the bursts we detect feature single-peaked lightcurves, also when inspecting 100–200 s around the peak with 1–4 s time resolution, and we find no signs of PRE in the GBM time resolved spectroscopy of any of the bursts (but see Sec. 4.1). The burst peak luminosities (L_{peak}) that we find range from 0.7×10^{38} erg s $^{-1}$ to 2.7×10^{38} erg s $^{-1}$ (Table 2). The rise times we measure in the GBM band (t_{rise} ; Sec. 2.1 for definition) are between 1 s and 5 s. By integrating the

bolometric luminosity over the fraction of the bursts detected by GBM, we find burst energies in the range $[0.4\text{--}5.8] \times 10^{39}$ erg. The burst duration in the GBM band was between 10 s and 50 s. Due to the combined effects of the GBM bandpass and background, these are lower limits to the total radiated burst energy and duration (see Section 4.1 for further discussion of bandpass corrections).

From the 15 bursts detected and the $\simeq 50\%$ observing duty cycle (Sec. 2.1), we find a burst recurrence time between March 2010 and March 2011 of $t_{\text{rec}} = 12 \pm 3$ d (1σ confidence interval from Poisson statistics). Notably, bursts B12 and B13 were only 2.8 d apart, the closest burst pair ever detected from 4U 0614+09 (shortest t_{wait} known to date was one week; K10). Four bursts were detected in January 2011 corresponding to a recurrence time of $\simeq 4$ d, shorter than the recurrence time during the preceding 10 months (t_{rec} was $\simeq 13$ d between 2010 March 12 and December 31). This can be seen in Figure 1, which shows the times of the bursts detected by GBM together with the \dot{m} evolution. Assuming a Poisson distribution, the probability of detecting at least 4 bursts during one month (effectively two weeks) for the average burst detection rate 1.3 month^{-1} (effectively 1.3 per 2 week-period) is 3.8%. This suggests that the intrinsic thermonuclear burst rate from 4U 0614+09 increased during January 2011. The source state during January 2011 was similar to the rest of the search period. The inferred \dot{m} reached a minimum near January 2011 (at $\dot{m}/\dot{m}_{\text{Edd}} \simeq 0.6\%$).

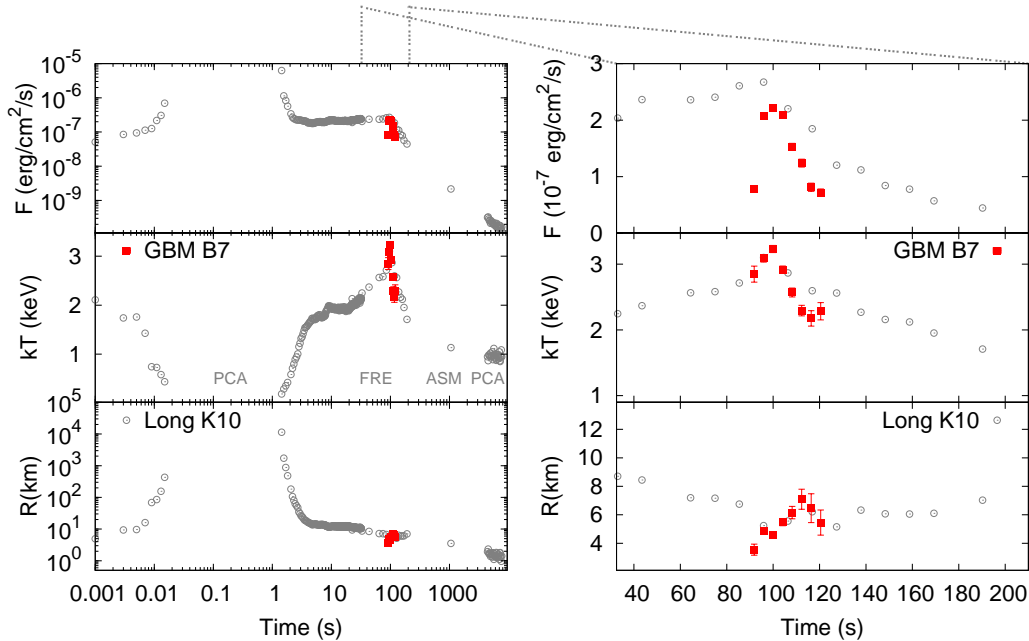


FIG. 5.— Spectral evolution during a long PRE burst from 4U 0614+09 detected in 2001 (open gray circles; from K10, burst FR 51944). Panels show, *from top to bottom*: bolometric flux, blackbody temperature and radius (for a distance of 3.2 kpc and without color or gravitational redshift corrections). We compare this to the spectral evolution measured by GBM during burst B7, detected in 2010 (filled red squares; see Tables 1 & 2). *Left* panels display the entire (about 8000 s long) long burst time range. *Right* panels zoom into the touchdown phase of the burst, the only part hot enough to be detected in the hard X-ray band (i.e., by GBM and FREGATE).

We do not detect long/intermediate bursts from 4U 0614+09 during the 1 yr search period, and we can place a 95% lower limit (assuming a Poisson distribution, Gehrels 1986) on the long burst recurrence time of 62 d. Our measurement of t_{rec} is consistent with previous estimates, which placed t_{rec} between one week and three months (in’t Zand et al. 2007; Kuulkers et al. 2010). Figure 4 compares t_{rec} from 4U 0614+09 as measured by several instruments during the last sixteen years, between 1996 and 2012. In only one year, the GBM results presented herein have provided the most accurate measurement of t_{rec} and revealed the shortest t_{wait} in 4U 0614+09. Furthermore, we are beginning to probe changes in t_{rec} on timescales of months, as illustrated by the likely increase in burst rate during January 2011.

4. DISCUSSION

We have presented the detection and properties of 15 thermonuclear bursts from 4U 0614+09 observed between March 2010 and March 2011 within our GBM all-sky search for X-ray bursts. Using only one year of GBM data we increased by 40% the sample of bursts from 4U 0614+09 collected over more than three decades (K10). These results illustrate the benefits of an X-ray monitor with instantaneous coverage of most ($\simeq 75\%$) of the sky and yield a robust measurement of the recurrence time of low- \dot{m} bursts in 4U 0614+09: $t_{\text{rec}} = 12 \pm 3$ d.

Figure 4 shows the full 1996–2012 ASM light curve (top panel; monthly-averaged intensity with error bars showing its standard deviation during each month) together with t_{rec} in 4U 0614+09. The average burst rate has been steady over 16 yr, with two marginal changes: a decrease in burst rate in 2001–2002 reported by K10, associated with lower variability in the ASM light curve, and the increased burst rate in January 2011 reported

herein. The two only known long/intermediate bursts from 4U 0614+09 happened in the 2001–2002 period, when the variability on long (days–months) timescales was at a minimum (Fig. 4). This “calm” period has not repeated ever since, which could explain why we do not detect long/intermediate bursts during 2010–2011.

4.1. Bandpass corrections: total burst energy and duration

The energy spectrum of thermonuclear bursts is for most purposes well described by a simple absorbed blackbody model. At the peak (near the flux maximum) bursts can show a wide variety of light curve shapes and spectral evolution. In particular, the peak of photospheric radius expansion (PRE) bursts features a drastic increase of the blackbody radius R_{bb} and an associated drop of the blackbody temperature kT_{bb} , due to the effect of radiation forces on the NS photosphere (e.g., Lewin et al. 1993, and references therein). Subsequently the photosphere contracts and heats up until it reaches the NS surface again, at “touchdown”. Most low- \dot{m} bursts are PRE events (of either normal or long duration class) as the high ignition depths power energetic and luminous events that can overcome the gravitational force at the photosphere.

Soft X-ray sensitivity is necessary in order to observe the full radius expansion phase of PRE bursts, due to the simultaneous drop in temperature which shifts the spectrum to lower energies. Conversely, the lack of spectroscopic evidence for PRE when observing a given burst in the hard X-ray band does not rule out the PRE nature of the burst. This is shown in Figure 5, where we compare the spectral evolution of a long PRE burst from 4U 0614+09 observed in 2001 with broadband spectral coverage (with the PCA, ASM and FREGATE instruments; from K10) to one of the GBM bursts pre-

TABLE 3
BANDPASS CORRECTIONS TO BURST ENERGY AND DURATION.

Burst	GBM (8–1000 keV)		FREGATE (6–400 keV)		PCA (2–60 keV)		FREGATE/GBM		PCA/GBM	
	E_{obs} (erg)	t_{obs} (s)	E_{obs} (erg)	t_{obs} (s)	E_{b} (erg)	t_{b} (s)	$E_{\text{obs}}/E_{\text{obs}}$	$t_{\text{obs}}/t_{\text{obs}}$	$E_{\text{b}}/E_{\text{obs}}$	$t_{\text{b}}/t_{\text{obs}}$
Normal (FR 52951)	3.6×10^{39}	30	6.0×10^{39}	45	?	?	1.7	1.5	>1.7	>1.5
Long (FR 51944)	3.4×10^{40}	140	3.9×10^{40}	308	4.4×10^{40}	7700	1.1	2.2	1.3	55

^aBurst energy and duration for a long and normal burst measured with three instruments in different energy bands, as indicated. PCA and FREGATE data are taken from K10. GBM values are obtained from simulated light curves (Sec. 4.1). PCA values are considered bolometric measurements of the burst energy and duration. Bandpass correction factors are given as ratios between the values measured in: FREGATE/GBM and PCA/GBM. Based on the last two columns we estimate the bolometric corrections on burst energy and duration as $E_{\text{b}}/E_{\text{obs}}=[1.3-1.7]$ and $t_{\text{obs}}/t_{\text{obs}}=[1.5-55]$, respectively (Sec. 4.1).

sented herein. In all cases except B3 and B13 the fluxes, temperatures and blackbody radii measured during our GBM bursts are consistent with those measured near the “touchdown” phase of a PRE burst (Figure 5 shows one example, B7). Thus most thermonuclear bursts detected with GBM (and perhaps with any hard X-ray wide field detector) are in fact consistent with PRE bursts in the touchdown phase. However, as our GBM X-ray burst search includes faint and untriggered events we are also sensitive to fainter, sub-Eddington bursts, as witnessed by the detection of B3 and B13 (Table 2 & Figure 3). All the GBM bursts presented herein are much shorter than the segment of the long burst detected by FREGATE. This, together with the simulations described below, indicates that all bursts B1–B15 are normal duration bursts, even after bandpass corrections are applied.

Due to its spectral evolution, a given burst can produce very different light curves when observed with instruments with different bandpasses (see, e.g., Chelovekov et al. 2006). This is of particular relevance when studying thermonuclear bursts with a hard X-ray detector, as many of the burst photons are emitted outside the energy range to which the instrument is sensitive to. Whenever a burst is clearly detected, its thermal spectrum is usually well constrained using the hard X-ray band and the bolometric flux can therefore be measured, under the assumption that color and effective temperatures are equal.

However, the actual burst detection relies on having sufficient burst photons emitted in the instrument band to rise significantly above the background rate. In practice, this implies that instruments like GBM (sensitive to photon energies above 8 keV; Meegan et al. 2009), FREGATE (sensitive above 6 keV; Atteia et al. 2003), BAT or IBIS-ISGRI (sensitive above 15 keV; Barthelmy et al. 2005; Lebrun et al. 2003, respectively) are able to detect only the hottest ($kT_{\text{bb}} \gtrsim 1.5-2$ keV) and relatively long-lived phases of bursts (see Figure 5). Thus in general the radiated energy and duration measured in the hard X-ray band (E_{obs} and t_{obs} , respectively) are lower limits to the total burst fluence and duration (E_{b} and t_{b}). This was illustrated by the long burst from XTE J1701–407 detected with both the XRT (sensitive in the 0.5–10 keV band) and BAT instruments onboard *Swift* (Linares et al. 2009). In that case E_{b} and t_{b} exceeded those measured in the BAT (15–50 keV) band by a factor of $E_{\text{b}}/E_{\text{obs}} \simeq 3.9$ and $t_{\text{b}}/t_{\text{obs}} \simeq 20$, respectively (Linares et al. 2009).

In order to quantify this combined bandpass and background effect for the GBM bursts from 4U 0614+09 and to estimate the total radiated energy and duration, we

simulated GBM light curves using two of the bursts reported by (K10): the long PRE burst shown in Figure 5 and a normal duration burst. We created a response matrix for one GBM NaI detector (n0, 14° off-axis; CTIME mode) and used the spectral parameters from both bursts (with a 10 s time resolution) to simulate net light curves within Xspec (v. 12.7.0; Arnaud 1996). We calculated count rates in the energy range 12–25 keV (CTIME channel 1), the band used in our systematic search (Sec. 2.1). We then added the net burst counts to a real background light curve which includes contributions from particle background and X-ray sources in the field of view, both variable typically on timescales $\gtrsim 100$ s. Finally, we measured the energy (from the integrated fluence, using the 3.2 kpc distance) and duration of each burst in the sub-interval detected by GBM.

The resulting simulated light curves are shown in Figure 6 (right panels). The long burst seen in the GBM band would present a characteristic slow rise ($t_{\text{rise}} \simeq 65$ s) and last for a total of about 140 s. The simulated normal duration burst, on the other hand, has a rise time (6.4 s), energy (3.6×10^{39} erg) and duration (30 s) similar to all GBM bursts presented herein (Table 2). This is shown in Figure 6 by comparing two of the GBM bursts (left panels; B4 & B8) with the simulated long and normal burst light curves (right panels). We conclude that all bursts detected from 4U 0614+09 during the first year of our GBM X-ray burst search are normal duration bursts, yet as discussed below they are more energetic than most normal duration bursts.

Table 3 presents the duration and energy of the long and normal duration bursts, as measured with three different instruments and bandpasses: GBM, FREGATE and PCA. The GBM values are estimated from the simulations explained above, while FREGATE and PCA values are taken from K10. The bolometric correction factors for energy and duration are given for each case. FREGATE was able to detect a slightly longer portion of the bursts. Although FREGATE also consisted of NaI scintillation detectors with effective area similar to that of the GBM detectors, its lower energy threshold (6 keV) and smaller field of view (which reduces X-ray background) made it sensitive to a larger fraction of the bursts.

The bandpass used has a clear effect on the measured burst energy, with $E_{\text{b}}/E_{\text{obs}}$ in the range 1.3–1.7 (1.3–4 if we include the XRT/BAT long burst from Linares et al. 2009). We note that the same is true for the commonly used characteristic burst timescale $E_{\text{b}}/L_{\text{peak}}$. The impact on the measured burst duration is much more drastic, as $t_{\text{b}}/t_{\text{obs}}$ can be anywhere between 1.5 and 55. This

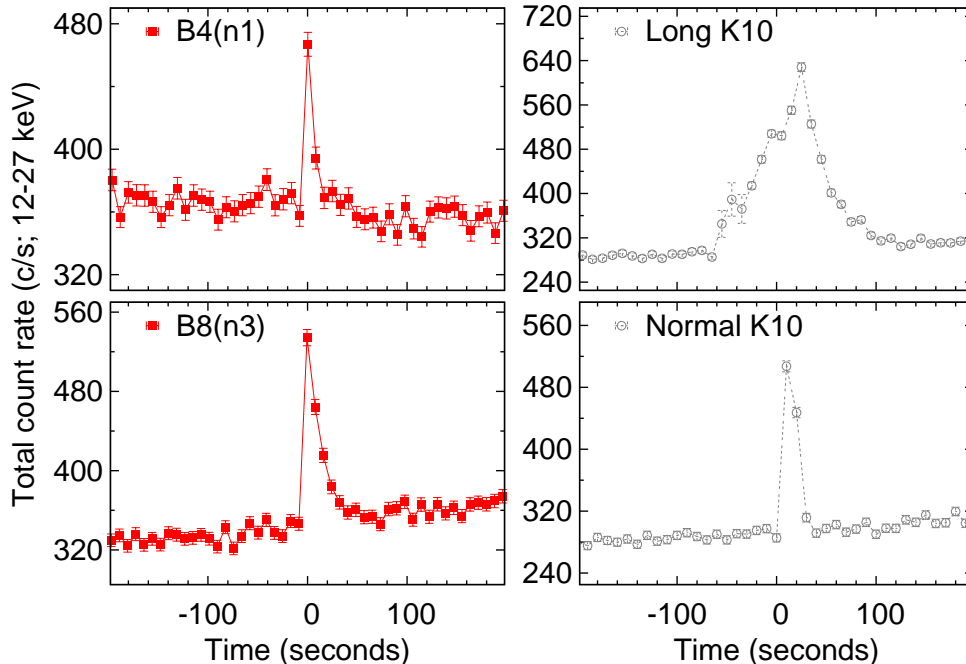


FIG. 6.— *Right panels:* Simulated GBM light curves in the 12-25 keV band at 10 s time resolution for a pointing offset of 14° , using the spectral evolution measured by HETE-FREGATE during a long (*top*) and normal duration (*bottom*) burst from 4U 0614+09 (both taken from K10). *Left panels:* Light curves for two of the GBM bursts from 4U 0614+09 reported herein, in the 12–25 keV band with 8 s time resolution and including background rate. In both cases the pointing offset was 14° ; detector number is indicated between parenthesis next to the burst ID (Tables 1 and 2).

is because cooling tails can extend for a long time (e.g.; in’t Zand et al. 2009) and are detected only with soft X-ray detectors, yet most of the energy is radiated during the hottest, most luminous phases of bursts which are captured to a greater extent by hard X-ray detectors. Thus in general burst energy constitutes a more robust (less band-dependent) observable than burst duration. As normal duration bursts from 4U 0614+09 have not been observed with pointed soft X-ray detectors, we cannot find the bolometric correction factors for the case of normal duration bursts from 4U 0614+09 observed with GBM. Based on our GBM simulation and the FREGATE normal duration burst, we estimate that in this case $E_b/E_{\text{obs}} \simeq 2$ (Table 3), i.e., normal bursts are about twice as energetic as seen in the GBM band.

4.2. 4U 0614+09 and low- \dot{m} bursts

In Figure 7 we compare the t_{rec} measured in 4U 0614+09, when \dot{m} was between 0.6% and 1.3%, to the constraints available for other low- \dot{m} bursters and a few selected systems. The $t_{\text{rec}}-\dot{m}$ relations for two “well-behaved” bursters accreting at a few percent of \dot{m}_{Edd} are shown for comparison (Galloway et al. 2004; Falanga et al. 2011). In those cases t_{rec} is shorter than a day and thus much easier to measure. For comparison, He ignition curves for pure He accretion are also shown, for two different values of the heat flux from the crust ($Q_b=1$ MeV/nucleon and $Q_b=3$ MeV/nucleon; see Cumming & Bildsten 2000, for details). The large change in predicted t_{rec} illustrates the sensitivity of low- \dot{m} bursts to the thermal properties of the crust. These models, however, predict burst energies much higher than the observed ones. Detailed modeling of the burst properties is beyond the scope of this work, and we refer

the reader to K10 for further discussion.

It is interesting to compare the distribution of burst energies from 4U 0614+09 with that of the normal duration and long/intermediate burst populations (see Figure 8). As discussed in Section 4.1, burst energy is less sensitive to bandpass effects than burst duration, and may constitute a more robust observable for burst classification. 4U 0614+09 has on average larger E_b than normal duration bursts, yet smaller E_b than long/intermediate duration bursts. The energies of the two long bursts from 4U 0614+09 (K10), however, are consistent with the rest of the long burst population. Even after bandpass effects are corrected for, 4U 0614+09 bridges the gap between normal duration and long/intermediate bursts (Fig. 8). This could be due to a fuel composition different than most ultracompact LMXBs that would give rise to atypical bursts, if as it has been suggested the donor star has unusual abundances (H and He deficient; Werner et al. 2006, see also Sec. 1).

Alternatively, the previously observed bimodal distribution of burst durations could be due to a selection effect. Prior to our GBM campaign, observations of low- \dot{m} bursts were mostly based on serendipitous detections with hard X-ray wide-field instruments. If such serendipitous and so far relatively scarce detections are biased towards the longest and most energetic events, a population of infrequent, low- \dot{m} bursts with energies and durations between normal and long bursts could have gone unnoticed. Our GBM all-sky search (Sec. 2.1) is the first systematic survey of low- \dot{m} bursts and is less biased towards long and energetic events. A continuous distribution in E_b (between 10^{39} erg and 10^{41} erg) is actually not surprising from the standpoint of He ignition models (Cumming & Bildsten 2000). This is, as far as we

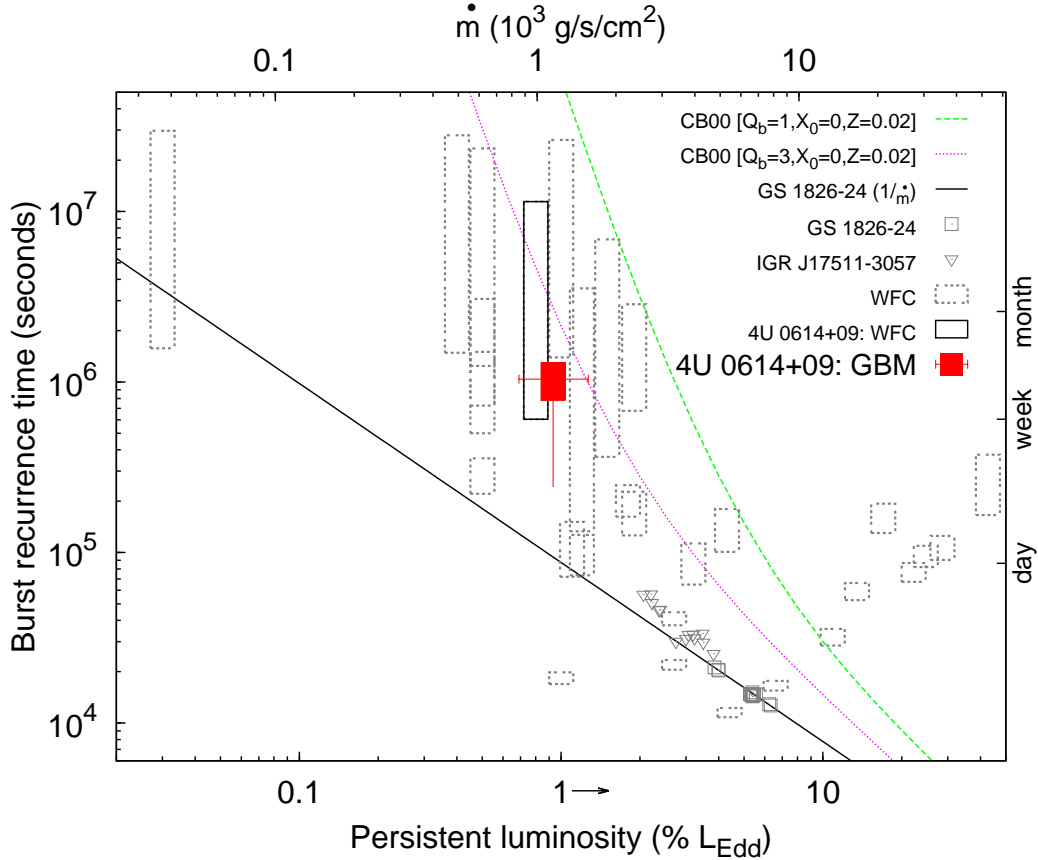


FIG. 7.— Burst recurrence time t_{rec} vs. persistent luminosity and inferred \dot{m} for 4U 0614+09 and a sample of bursters. The red filled rectangle shows the GBM measurement (1σ confidence interval) of the average t_{rec} in 4U 0614+09. The red vertical error bar corresponds to the shortest wait time between bursts that we find, 2.8 d, and the horizontal error bars show the range in L_{pers} and \dot{m} . Open (gray dashed) rectangles show the 1σ confidence intervals obtained from 6 yr of WFC data, taken from in't Zand et al. (2007, only systems below 50% L_{Edd} are shown). The solid open black rectangle shows the WFC limits on t_{rec} for 4U 0614+09. Open squares and triangles show t_{rec} measurements in GS 1826-24 (Galloway et al. 2004) and IGR J17511-3057 (Falanga et al. 2011), respectively. The solid black line shows the $t_{\text{rec}} \propto 1/\dot{m}$ relation found by Galloway et al. (2004) for GS 1826-24. Green dashed and purple dotted lines show the $t_{\text{rec}}(\dot{m})$ relation predicted by He ignition models (Cumming & Bildsten 2000, for pure He accretion and solar metallicity) for a base heat flux of 1 MeV/nucleon and 3 MeV/nucleon, respectively. The arrow below the bottom axis shows the change on the Eddington fraction if a value of $L_{\text{Edd}} = 3.8 \times 10^{38}$ erg s $^{-1}$ is used (Sec. 2.4).

know, the first time that such continuous distribution is observed. Extending this study to similar bursters will determine if the distribution of burst energies that we find (Figure 8) is unique to 4U 0614+09 or a common feature of low- \dot{m} bursters.

The average burst energy in our sample, after the bolometric correction factor of $\simeq 2$ is applied (Sec. 4.1), is 5×10^{39} erg. For the measured t_{rec} (12 d) and L_{pers} (2.3×10^{36} erg s $^{-1}$), this corresponds to an accretion-to-burst fluence ratio $\alpha \simeq 560$, while the accreted column depth at the average inferred \dot{m} (1.1×10^3 g cm $^{-2}$ s $^{-1}$) is $y \simeq 1 \times 10^9$ g cm $^{-2}$, similar to the values obtained from light curve fitting (2×10^9 g cm $^{-2}$ for the normal duration burst in K10). However, complete ignition of such a thick layer would give rise to more energetic bursts than observed, assuming the energy release expected for pure He burning (as discussed by K10). For the shortest t_{wait} burst (B13), using the average L_{pers} and \dot{m} during January 2011 (1.8×10^{36} erg s $^{-1}$ and 0.9×10^3 g cm $^{-2}$ s $^{-1}$, respectively) yields a similarly high value of $\alpha \simeq 506$. This indicates that even the shortest t_{rec} bursts in 4U 0614+09 are sub-energetic. Thus after our improved t_{rec} measurements and considering bolometric/bandpass corrections

to E_b , the question of why are most bursts in 4U 0614+09 sub-energetic remains open. We also note that the shortest t_{wait} burst (B13) has the lowest E_b in our sample, as expected if the mass accumulated before ignition is also lowest. We found the period with the shortest t_{rec} near the minimum in \dot{m} (Sec. 3). This behavior is opposite to what ignition models predict and it might be due to different rates of stable H (CNO) burning operating at slightly different \dot{m} (although the apparent lack of H in the fuel makes this scenario unlikely). Alternatively, it could reflect changes in the $L_{\text{pers}}-\dot{m}$ relation (i.e., in the radiative efficiency of the accretion flow) unaccounted for. Continued monitoring may determine whether this is a weeks-long fluctuation in the observed burst rate or it constitutes a systematic behavior of 4U 0614+09.

As can be seen in Figure 7, our GBM campaign in its first year has improved the accuracy of t_{rec} measurements at low \dot{m} , placing new constraints on models of low- \dot{m} ignition. Most estimates available to date were based on *BeppoSAX*-WFC observations and provided mostly order-of-magnitude constraints on t_{rec} (Fig. 7). Extending our GBM measurements to other low- \dot{m} bursters and comparing them to theoretical models, considering po-

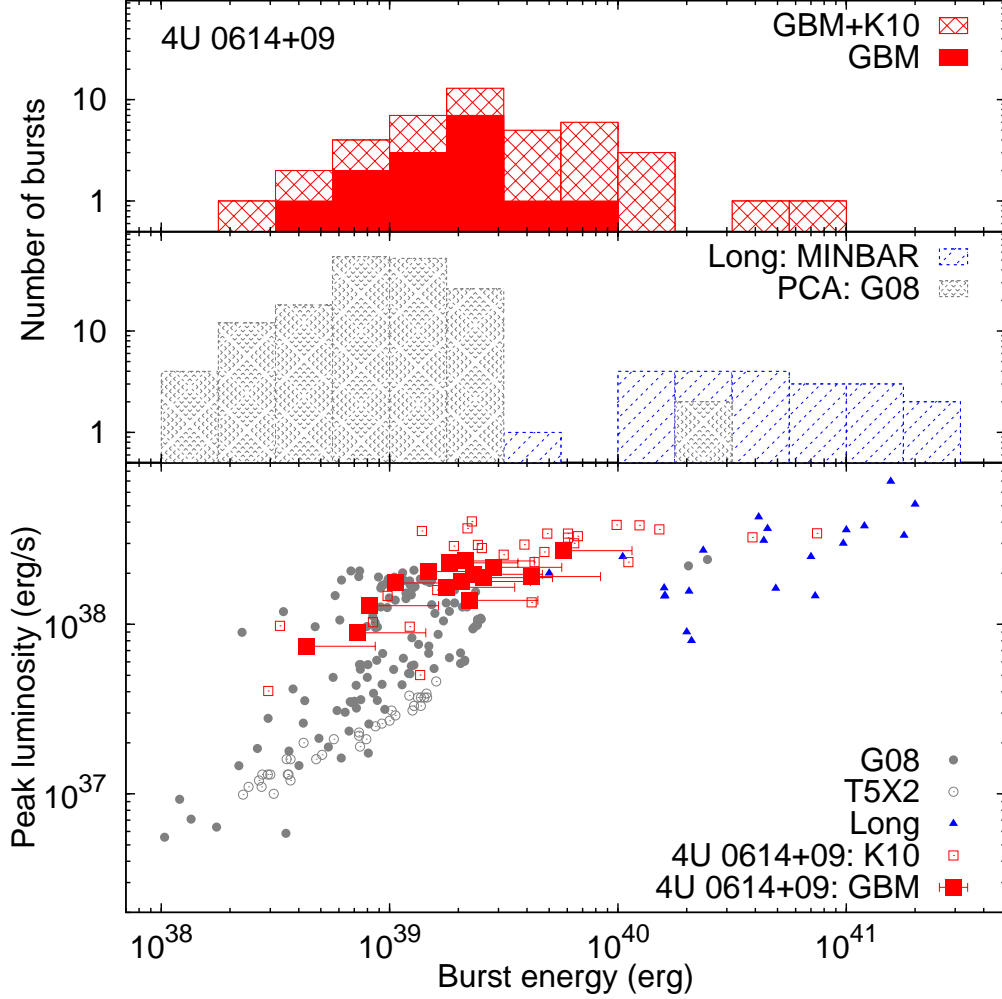


FIG. 8.— *Bottom*: Burst peak luminosity vs. energy, for the GBM bursts from 4U 0614+09 presented herein (filled red squares; error bars show estimated bolometric correction factor, see Sec. 4.1), for all known bursts from 4U 0614+09 including those reported in K10 (open red squares), for all bursts from the *RXTE* catalog (filled gray circles, Galloway et al. 2008), for the 11 Hz pulsar in the globular cluster Terzan 5 (open gray circles, Linares et al. 2012) and for the long/intermediate bursts from the MINBAR catalog (filled blue triangles). *Middle and top panels*: Histograms showing the number of bursts per energy bin for the different known samples, as indicated. 4U 0614+09 bridges the gap between the “normal” and “long/intermediate” burst populations (Sec 4.2).

tential changes in fuel composition across bursters, can make precise measurements of crustal heat flux possible.

5. SUMMARY

- We have presented 15 normal duration thermonuclear bursts from 4U 0614+09 observed with *Fermi*-GBM between March 2010 and March 2011, when the source was accreting near 1% of the Eddington rate. We measured a burst recurrence time of 12 ± 3 d and find the closest burst pair seen from 4U 0614+09 to date, 2.8 d apart.
- We find no long/intermediate bursts in one year of data, and set a lower limit to their recurrence time of 62 d. The 2001–2002 “calm” (low long-term variability) period in the persistent soft X-ray emission during which long/intermediate bursts were detected has not recurred.
- We quantify the bandpass effect on the observed burst duration and energy. We find that the total burst duration can be 1.5–55 times longer than that measured

in the hard X-ray band, whereas this bolometric correction factor is 1.3–1.7 for burst energy (which is therefore a more robust, band-independent observable).

- The burst energies in 4U 0614+09, between 8×10^{38} erg and 1×10^{40} erg after our bolometric correction is applied, overlap between the energies of the normal and long burst populations. This continuous distribution in burst energy provides new observational evidence that long/intermediate bursts are an extreme case of low- \dot{m} bursts. We suggest that the apparent bimodal distribution of durations that defined normal and long/intermediate bursts could be due to a selection effect if only the longest and most energetic low- \dot{m} bursts could be detected to date.

Acknowledgments: Quick-look ASM results were provided by the *RXTE*/ASM team. Swift/BAT transient monitor results were provided by the Swift/BAT team. This paper utilizes preliminary analysis results from the Multi-INstrument Burst ARchive (MINBAR; <http://users.monash.edu.au/~dgallo/minbar>). Data

from previous bursts were kindly provided by E. Kuulkers. We thank A. Cumming for providing ignition models and for stimulating discussions and V. Chaplin for clarifications on detector geometries during some of the bursts. We also thank the anonymous referee for constructive

comments. ML is grateful to the International Space Science Institute in Bern, where part of this work was completed, and acknowledges support from the NWO Rubicon fellowship. This research was partly funded by NASA's Fermi Guest Investigation program under grant NNX11AO19G.

REFERENCES

- Arnaud, K. A. 1996, in *Astronomical Society of the Pacific Conference Series*, Vol. 101, *Astronomical Data Analysis Software and Systems V*, ed. G. H. Jacoby & J. Barnes, 17–+
- Atteia, J.-L., et al. 2003, in *American Institute of Physics Conference Series*, Vol. 662, *Gamma-Ray Burst and Afterglow Astronomy 2001: A Workshop Celebrating the First Year of the HETE Mission*, ed. G. R. Ricker & R. K. Vanderspek, 17–24
- Barthelmy, S. D., et al. 2005, *Space Science Reviews*, 120, 143
- Brandt, S., Castro-Tirado, A. J., Lund, N., Dremmin, V., Lapshov, I., & Syunyaev, R. 1992, *A&A*, 262, L15+
- Chelovekov, I. V., Grebenev, S. A., & Sunyaev, R. A. 2006, *Astronomy Letters*, 32, 456
- Chenevez, J., Falanga, M., Kuulkers, E., Brandt, S., Lund, N., & Cumming, A. 2008, in *Proceedings of the 7th INTEGRAL Workshop*
- Coriat, M., Fender, R. P., & Dubus, G. 2012, *ArXiv e-prints*
- Cornelisse, R., Heise, J., Kuulkers, E., Verbunt, F., & in't Zand, J. J. M. 2000, *A&A*, 357, L21
- Cumming, A., & Bildsten, L. 2000, *ApJ*, 544, 453
- Cumming, A., Macbeth, J., in't Zand, J. J. M., & Page, D. 2006, *ApJ*, 646, 429
- Falanga, M., et al. 2011, *A&A*, 529, A68+
- Galloway, D. K., Cumming, A., Kuulkers, E., Bildsten, L., Chakrabarty, D., & Rothschild, R. E. 2004, *ApJ*, 601, 466
- Galloway, D. K., Muno, M. P., Hartman, J. M., Psaltis, D., & Chakrabarty, D. 2008, *ApJS*, 179, 360
- Gehrels, N. 1986, *ApJ*, 303, 336
- Giacconi, R., Murray, S., Gursky, H., Kellogg, E., Schreier, E., & Tananbaum, H. 1972, *ApJ*, 178, 281
- Grindlay, J., Gursky, H., Schnopper, H., Parsignault, D. R., Heise, J., Brinkman, A. C., & Schrijver, J. 1976, *ApJ*, 205, L127
- Hasinger, G., & van der Klis, M. 1989, *A&A*, 225, 79
- in't Zand, J. J. M., Cumming, A., van der Sluys, M. V., Verbunt, F., & Pols, O. R. 2005, *A&A*, 441, 675
- in't Zand, J. J. M., Jonker, P. G., & Markwardt, C. B. 2007, *A&A*, 465, 953
- in't Zand, J. J. M., Keek, L., Cumming, A., Heger, A., Homan, J., & Méndez, M. 2009, *A&A*, 497, 469
- Juett, A. M., Psaltis, D., & Chakrabarty, D. 2001, *ApJ*, 560, L59
- Krimm, H. A., Barthelmy, S. D., Markwardt, C. B., Sanwal, D., Tueller, J., Gehrels, N., & Swift/BAT Team. 2006, in *Bulletin of the American Astronomical Society*, Vol. 38, *AAS/High Energy Astrophysics Division #9*, 374
- Kuulkers, E. 2004, *Nuclear Physics B Proceedings Supplements*, 132, 466
- Kuulkers, E., et al. 2010, *A&A*, 514, A65+
- Lebrun, F., et al. 2003, *A&A*, 411, L141
- Levine, A. M., Bradt, H., Cui, W., Jernigan, J. G., Morgan, E. H., Remillard, R., Shirey, R. E., & Smith, D. A. 1996, *ApJ*, 469, L33+
- Lewin, W. H. G., van Paradijs, J., & Taam, R. E. 1993, *Space Science Reviews*, 62, 223
- Linares, M. 2009, PhD thesis, *Sterrenkundig Instituut "Anton Pannekoek" - University of Amsterdam*
- Linares, M., Altamirano, D., Chakrabarty, D., Cumming, A., & Keek, L. 2012, *ApJ*, 748, 82
- Linares, M., Watts, A. L., Wijnands, R., Soleri, P., Degenaar, N., Curran, P. A., Starling, R. L. C., & van der Klis, M. 2009, *MNRAS*, 392, L11
- Maraschi, L., & Cavaliere, A. 1977, in *X-ray Binaries and Compact Objects*, ed. K. A. van der Hucht, 127–128
- Meegan, C., et al. 2009, *ApJ*, 702, 791
- Migliari, S., Tomsick, J. A., Maccarone, T. J., Gallo, E., Fender, R. P., Nelemans, G., & Russell, D. M. 2006, *ApJ*, 643, L41
- Nelemans, G., Jonker, P. G., Marsh, T. R., & van der Klis, M. 2004, *MNRAS*, 348, L7
- O'Brien, K., Rodriguez, Jonker, Dhillon, Nelemans, Marsh, Still, & van der Klis, M. 2005, Poster at symposium "A life with stars", Amsterdam, 1, 1
- Peng, F., Brown, E. F., & Truran, J. W. 2007, *ApJ*, 654, 1022
- Shahbaz, T., Watson, C. A., Zurita, C., Villaver, E., & Hernandez-Peralta, H. 2008, *PASP*, 120, 848
- Strohmayer, T., & Bildsten, L. 2006, *New views of thermonuclear bursts*, ed. W. H. G. Lewin & M. van der Klis, 113–156
- Swank, J. H., Boldt, E. A., Holt, S. S., Serlemitsos, P. J., & Becker, R. H. 1978, *MNRAS*, 182, 349
- van Paradijs, J., & McClintock, J. E. 1994, *A&A*, 290, 133
- Werner, K., Nagel, T., Rauch, T., Hammer, N. J., & Dreizler, S. 2006, *A&A*, 450, 725